Development/Plasticity/Repair

Spatiotemporal Developmental Gradient of Thalamic Morphology, Microstructure, and Connectivity from the Third Trimester to Early Infancy

Weihao Zheng,[1,2] Leilei Zhao,[2] Zhiyong Zhao,[1] Tingting Liu,[1] Bin Hu,[3] and Dan Wu[1,4]

[1]Key Laboratory for Biomedical Engineering of Ministry of Education, College of Biomedical Engineering and Instrument Science, Zhejiang University, Hangzhou 310027, People's Republic of China, [2]Gansu Provincial Key Laboratory of Wearable Computing, School of Information Science and Engineering, Lanzhou University, Lanzhou 730000, People's Republic of China, [3]School of Medical Technology, Beijing Institute of Technology, Beijing 100081, People's Republic of China, and [4]Binjiang Institute, Zhejiang University, Hangzhou 310053, People's Republic of China

Thalamus is a critical component of the limbic system that is extensively involved in both basic and high-order brain functions. However, how the thalamic structure and function develops at macroscopic and microscopic scales during the perinatal period development is not yet well characterized. Here, we used multishell high-angular resolution diffusion MRI of 144 preterm-born and full-term infants in both sexes scanned at 32–44 postmenstrual weeks (PMWs) from the Developing Human Connectome Project database to investigate the thalamic development in morphology, microstructure, associated connectivity, and subnucleus division. We found evident anatomic expansion and linear increases of fiber integrity in the lateral side of thalamus compared with the medial part. The tractography results indicated that thalamic connection to the frontal cortex developed later than the other thalamocortical connections (parieto-occipital, motor, somatosensory, and temporal). Using a connectivity-based segmentation strategy, we revealed that functional partitions of thalamic subdivisions were formed at 32 PMWs or earlier, and the partition developed toward the adult pattern in a lateral-to-medial pattern. Collectively, these findings revealed faster development of the lateral thalamus than the central part as well as a posterior-to-anterior developmental gradient of thalamocortical connectivity from the third trimester to early infancy.

Key words: **diffusion MRI; early development; microstructure; subdivisions; thalamocortical connectivity; thalamus**

Significance Statement

This is the first study that characterizes the spatiotemporal developmental pattern of thalamus during the third trimester to early infancy. We found that thalamus develops in a lateral-to-medial pattern for both thalamic microstructures and subdivisions; and thalamocortical connectivity develops in a posterior-to-anterior gradient that thalamofrontal connectivity appears later than the other thalamocortical connections. These findings may enrich our understanding of the developmental principles of thalamus and provide references for the atypical brain growth in neurodevelopmental disorders.

Introduction

Thalamus is considered to be a "relay station" between perception cortices and high-order cortical associates. It receives sensation and perception inputs from sensory receptors and projects them to corresponding cortices via nerve fibers for subsequent processing. Thalamus has been characterized as a large collection of nuclei. Each nucleus connects with a specific cortical area and is responsible for the relay of unique information, such as lateral geniculate nucleus for vision, medial geniculate nuclei for auditory input, and ventral–posterior nucleus for the perception of touch and pain (Dostrovsky, 2000; Ward, 2013; Torrico and Munakomi, 2021). On the other hand, thalamus receives feedback from the cerebral cortex and is thus assumed to be extensively involved in modulating high-order brain functions, including attention, emotion, and consciousness (Mumford, 1991; Ward, 2011, 2013). Despite its critical role, thalamus remains one of the least understood regions in the brain. Understanding the developmental processes of thalamic structure may be of great importance for elucidating the fundamental mechanism of thalamic functional diversification.

Received May 8, 2022; revised Oct. 19, 2022; accepted Nov. 26, 2022.

Author contributions: W.Z., B.H., and D.W. designed research; W.Z., L.Z., Z.Z., T.L., B.H., and D.W. performed research; W.Z., L.Z., and T.L. analyzed data; W.Z., Z.Z., and D.W. wrote the paper.

This work was supported in part by the Ministry of Science and Technology of China (Grants 2018YFE0114600, 2021ZD0202002, 2021ZD0200800, and 2021ZD0200202,), and the National Natural Science Foundation of China (Grants 62202212, 82122032, and 81971606). We thank the numerous contributors to the dHCP database for their effort in the collection, organization, and sharing of their datasets.

The authors declare no competing financial interests.

Correspondence should be addressed to Dan Wu at danwu.bme@zju.edu.cn or Bin Hu at bh@lzu.edu.cn.

https://doi.org/10.1523/JNEUROSCI.0874-22.2022

Magnetic resonance imaging (MRI) provides a noninvasive neuroimaging tool to capture the dynamic process of early brain development. Compared with T1-weighted (T1w) and T2w images that have weak contrast for premature brains because of insufficient myelination, diffusion MRI (dMRI) has been extensively used to characterize the developing fetal and neonatal brains, given its superior contrasts in the immature brains and capability of resolving the early brain connections (Huang et al., 2006, 2009; Vasung et al., 2010; Takahashi et al., 2012; Song et al., 2015). Using dMRI-based tractography, studies have revealed that major fiber tracts (e.g., cingulum and inferior longitudinal fasciculus) formed at the end of the second trimester (Song et al., 2015; Feng et al., 2019; Machado-Rivas et al., 2021) and developed in a well defined pattern (Jaimes et al., 2020; Wilson et al., 2021). In addition, dMRI provides unique insights into the microstructural development of the perinatal brain, such as nonlinear changes of fractional anisotropy (FA; which declined until around 38 weeks), diffusivity, and diffusion kurtosis across the cortex (Ball et al., 2013a; Ouyang et al., 2019) and subcortical nuclei (Ball et al., 2012). Also, based on dMRI, several studies have segmented thalamus of the adult brain into stable and reproducible subdivisions through thalamocortical connections (Behrens et al., 2003; Jaimes et al., 2018; Zheng et al., 2021), which potentially can be replicated in the developing brains.

Thalamocortical system in developing brains during early infancy has attracted a lot of attention. It has been shown that both structural and functional thalamocortical connectivity of infants at term can predict cognitive and motor functions at 2 years old (Ball et al., 2015; Toulmin et al., 2021), suggesting that the development of the thalamocortical circuitry during the perinatal period is crucial for later neurocognitive functioning. On the other hand, some studies focused on the topographical segmentation of the thalamus in early infancy and demonstrated that structural and functional thalamocortical connectivity of infants at full-term age can yield subfields that correspond well to known thalamic anatomy (Toulmin et al., 2015; Jaimes et al., 2018); they also indicated that the thalamic parcellation might be modulated by various factors, such as prematurity and congenital heart disease. These studies demonstrated the significance of depicting the developmental process of the thalamocortical system during the perinatal period (e.g., third trimester and neonatal stage), which, however, remains a largely uncharted territory, and how the functional subdivisions of thalamus form during early development is unknown.

In the present study, we aimed to delineate the spatiotemporal developmental pattern of the thalamus and its association with the cerebral cortex during the perinatal period, using dMRI data of 144 preterm-born and term-born infants scanned from 32–44 PMWs in the Developing Human Connectome Project (dHCP) database (http://www.developingconnectome.org). We characterized the cross-sectional and longitudinal age-dependent developmental pattern of the thalamus in terms of its morphology, microstructures, and subdivisions, as well as the thalamocortical connectivity profiles, to provide a comprehensive picture of the developing thalamus in the early human brain.

Materials and Methods

Participants

Infants included in this study were recruited as a part of the dHCP database (second data release). The dHCP is an open science program approved by the United Kingdom Health Research Ethics Authority (reference no. 14/LO/1169). MR images and basic demographic data are available at http://www.developingconnectome.org, and written consent was obtained from all participating families before the scan.

The second release of dHCP contains 512 infant images, which underwent quality control using the dHCP EDDY QC tools (Bastiani et al., 2019a). To better characterize the developmental trajectory of thalamus and thalamocortical circuitry, relatively strict exclusion criteria were applied (Fig. 1). Specifically, we only included the first scan of each infant. The exclusion criteria were as follows: (1) infants who had no complete dMRI data ($n = 6$); (2) absence of basic information ($n = 3$); (3) a scan beyond the range of 32–44 PMWs ($n = 14$); (4) use of sedation during a scan ($n = 5$); (5) focal abnormality (radiology score > 3, $n = 36$); (6) low birth weight ($n = 16$); (7) images with $>5\%$ outlier slices or absolute motion >3 (evaluated through dHCP QC reports; $n = 139$); (8) ghosting artifact (evaluated through visual check, $n = 38$); and (9) one of twin data ($n = 12$). Only 175 subjects were left after the aforementioned steps, and most of them were scanned between 37 and 42 PMWs. To balance the data distribution, the following extra exclusion criteria were made for infants who were scanned after term age (37 PMWs): (10) infants who were born before 37 gestational weeks and scanned between 37 and 44 PMWs ($n = 14$); (11) infants who were scanned >1 week after birth with a scan age between 37 and 41 PMWs ($n = 15$); and (12) infants who were born before 39 gestational weeks and scanned between 42 and 44 PMWs ($n = 2$). This procedure resulted in the final cohort of 144 infants. We categorized these neonates into 13 groups according to their PMW at scan. The demographic information is provided in Table 1.

Image acquisition

Images were acquired on a 3 tesla Philips Achieva scanner equipped with a 32-channel neonatal head coil and a neonatal positioning device (Hughes et al., 2017) according to the dHCP protocol (http://www.developingconnectome.org). Neonates were asleep naturally during the scan. High-angular resolution multishell dMRI with a spherically optimized set of directions over 4 b-shells (20 b = 0 s/mm^2 images; b = 400 s/mm^2, 64 directions; b = 1000 s/mm^2, 88 directions; b = 2600 s/mm^2, 128 directions) were obtained. Other imaging parameters included the following: repetition time (TR) = 3800 ms; echo time (TE) = 90 ms; SENSE (sensitivity encoding) factor = 1.2; multiband acceleration factor = 4; in-plane resolution of 1.5 × 1.5 mm; and slice thickness of 3 mm with 1.5 mm slice overlap. T2w images were acquired using multislice fast spin-echo sequence with TR/TE = 12,000/156 ms, flip angle = 90, in-plane resolution = 0.8 × 0.8 mm, and slice thickness of 1.6 mm with a 0.8 mm overlap.

Image preprocessing

Preprocessing and tensor-based analysis. Images were preprocessed via the dHCP diffusion image-processing pipeline (Bastiani et al., 2019b). The preprocessing steps included intrasubject volume registration (Jenkinson et al., 2002), distortion correction, and eddy current correction using "TOPUP" and "EDDY" tools in FSL (Andersson et al., 2003; Andersson and Sotiropoulos, 2016; Andersson et al., 2017), and super-resolution reconstruction to achieve isotropic resolution of 1.5 mm (Kuklisova-Murgasova et al., 2012). FA, mean diffusivity (MD), radial diffusivity (RD), and axial diffusivity (AD) were then calculated based on the diffusion tensors.

Fixel-based analysis. The preprocessing of multishell dMRI was performed using MRtrix3 (www.mrtrix.org). Multishell multitissue (three tissues) constrained spherical deconvolution algorithm was applied to compute the fiber orientation distributions (FODs) in the spherical harmonic basis (Jeurissen et al., 2014). This approach addresses the challenge of resolving crossing fibers within a voxel and, thus, enables more accurate fiber tracking than the tensor model. A population template was generated from FOD images of all subjects through iterative registration and averaging. Because the brain grows rapidly during the perinatal period, we further generated a FOD template for each PMW. FOD images of all subjects were registered to the population template for fixel estimation, where fixels refer to fiber components within a voxel. Apparent fiber density (FD) and fiber-bundle cross-section (FC)

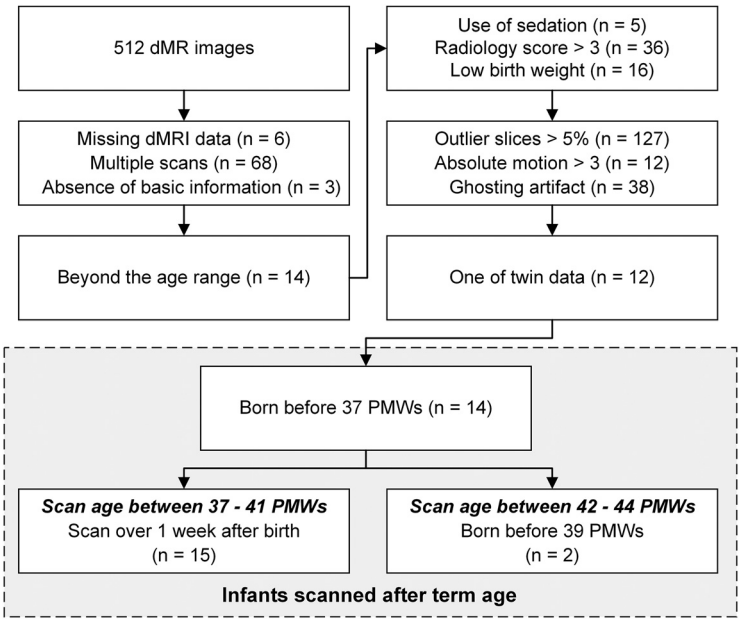

Figure 1. Flowchart for the subject exclusion procedure used in the present study.

Table 1. Demographic information of infants included in this study

Group	Gestational age (weeks)	Scan age (weeks)	Gender (M/F)	Head circumference at birth (cm)	Birth weight (kg)	Singleton/twins[a]
32 weeks	30.36 ± 1.74	32.61 ± 0.32	1/3	27.25 ± 0.50	1.27 ± 0.11	4/0
33 weeks	30.43 ± 2.16	33.39 ± 0.14	3/1	28.65 ± 0.85	1.28 ± 0.18	3/1
34 weeks	32.82 ± 1.31	34.55 ± 0.36	5/2	30.21 ± 0.27	2.14 ± 0.79	5/2
35 weeks	34.36 ± 1.15	35.48 ± 0.27	5/6	31.13 ± 1.08	2.08 ± 0.31	3/8
36 weeks	35.88 ± 0.46	36.59 ± 0.25	4/2	32.12 ± 0.81	2.39 ± 0.16	2/4
37 weeks	37.05 ± 0.28	37.46 ± 0.33	6/3	33.50 ± 0.94	2.73 ± 0.23	6/3
38 weeks	37.93 ± 0.50	38.42 ± 0.31	10/4	33.61 ± 0.92	2.88 ± 0.38	8/6
39 weeks	39.01 ± 0.49	39.43 ± 0.26	10/10	34.22 ± 0.81	3.15 ± 0.36	20/0
40 weeks	40.12 ± 0.39	40.56 ± 0.21	9/9	34.72 ± 0.69	3.33 ± 0.32	18/0
41 weeks	40.58 ± 0.85	41.41 ± 0.29	12/9	35.18 ± 0.80	3.41 ± 0.43	21/0
42 weeks	40.97 ± 0.80	42.23 ± 0.25	4/6	34.87 ± 0.89	3.49 ± 0.19	10/0
43 weeks	40.86 ± 0.57	43.53 ± 0.27	5/9	36.37 ± 0.49	3.46 ± 0.29	14/0
44 weeks	40.60 ± 0.40	44.36 ± 0.22	3/3	36.90 ± 1.06	3.30 ± 0.31	6/0

M, Male; F, female.
[a]Only one of the twins were used.

Table 2. Demographic information of infants included in the longitudinal study

Clinical characteristics	PB-AB	PB-TEA	TB
Gestational age (weeks)	32.43 ± 2.86		39.98 ± 1.21
Scan age (weeks)	34.57 ± 1.60	41.29 ± 1.47	41.29 ± 1.45
Gender: male/female	17/11		17/11
Birth weight (kg)	1.80 ± 0.69		3.44 ± 0.56
Head circumference at birth (cm)	30.09 ± 2.55	35.29 ± 1.66	35.38 ± 1.24
Singleton/twins	18/10		28/0

PB-AB, preterm-born after birth; PB-TEA, preterm-born at term-equivalent age; TB, term-born.

that reflects the intra-axonal property and fiber-bundle morphology, respectively, were calculated from the pipeline (Raffelt et al., 2017).

Thalamus segmentation. Each brain was segmented into 87 regions according to the DRAW-EM atlas based on the T2w image (Makropoulos et al., 2014). For each subject, the T2w image was aligned to the b = 0 s/mm^2 images of the dMRI data via boundary-based registration (Jenkinson et al., 2002; Greve and Fischl, 2009), and the transformation parameters with the nearest-neighbor interpolation were then applied to transform the parcellation map to the native dMRI space. We merged the high-intensity and low-intensity thalamic subfields of the DRAW-EM atlas to generate the mask of the whole thalamus.

Shape analysis of the thalamus

The deformation field of the thalamus was estimated by registering the individual thalamus to the thalamus in the population template of 40 PMWs through a FOD-guided nonlinear registration algorithm (Raffelt et al., 2011, 2012). This algorithm used the high-contrast and high-dimensional FOD to improve the alignment of local microstructures. This step allowed a direct comparison of the thalamic morphology at each time point with the 40 PMWs reference. We used the logarithm of the Jacobian determinant (J) of the nonlinear transformation matrix to represent the deformation (Zheng et al., 2021), with $J > 0$ indicating a shape expansion from the subject to the reference image and $J < 0$ indicating the opposite deformations. The thalamic shape change at the population level was calculated by transforming the FOD template at each PMW to the 40 PMWs template.

Thalamocortical connectivity

To investigate the developmental trajectory of thalamocortical fiber tracts during the perinatal period, a deterministic fiber-tracking algorithm based on the FOD image was applied to derive white matter tracts between cortex and thalamus (Tournier et al., 2012). This approach was suggested to provide more accurate connectome reconstruction for *in vivo* dMRI data than probabilistic algorithms (Sarwar et al., 2019). Twenty thousand streamlines were generated with seed voxels randomly selected across the thalamus using the following parameters: step size = 0.15 mm; maximum tracing angle = 22.5°; minimum/maximum fiber length = 5 mm/200 mm; and cutoff = 0.04. Densities of the thalamocortical tracts were mapped back to the thalamus for visualization of the spatial pattern of cortical projections across the thalamus.

Identification of thalamic subdivisions

The thalamic subdivisions were identified using a connectivity-based approach (Behrens et al., 2003). The UNC Neonatal Atlas (Shi et al., 2011) was registered to the FOD template at each PMW to create cortical parcellations, which were then reorganized into five cortical seed regions (i.e., frontal, motor, somatosensory, parietal-occipital, and temporal cortices) according to previous literature (Nair et al., 2013; Zheng et al., 2021). A probabilistic fiber-tracking algorithm (iFOD2) based on the second-order integration over FODs was applied to derive fiber tracts originating from the cortical seeds and terminating in thalamus (Tournier et al., 2010), with 5000 streamline samples for each cortical seed region. The tracking parameters were similar to those in the Thalamocortical connectivity subsection. Note probabilistic fiber tracking was used here considering the low anisotropy in cortical seed regions, similar to other works for connectivity-based segmentation (Behrens et al., 2003; Nair et al., 2013). The identification of thalamic subdivisions followed the "winner-take-all" principle that categorized each thalamic voxel according to the cortical seed region with the maximum streamlines to it.

Longitudinal analysis

To examine (1) the validity of our findings on thalamic development and (2) the effect of preterm-birth [e.g., whether the thalamic features we found in preterm-born (PB) at term-equivalent age (TEA) are comparable to healthy term-born (TB) infants], a validation analysis was performed on a longitudinal subset of dHCP. This dataset included PB subjects who were scanned twice several days after birth (PB-AB) and at TEA (PB-TEA). The first eight exclusion criteria in the Participants subsection were applied [except for steps 3 and 7, as they largely reduced the usable samples (only 11 subjects were left)]. The final dataset included 28 PB neonates and 28 TB infants who had matched gender,

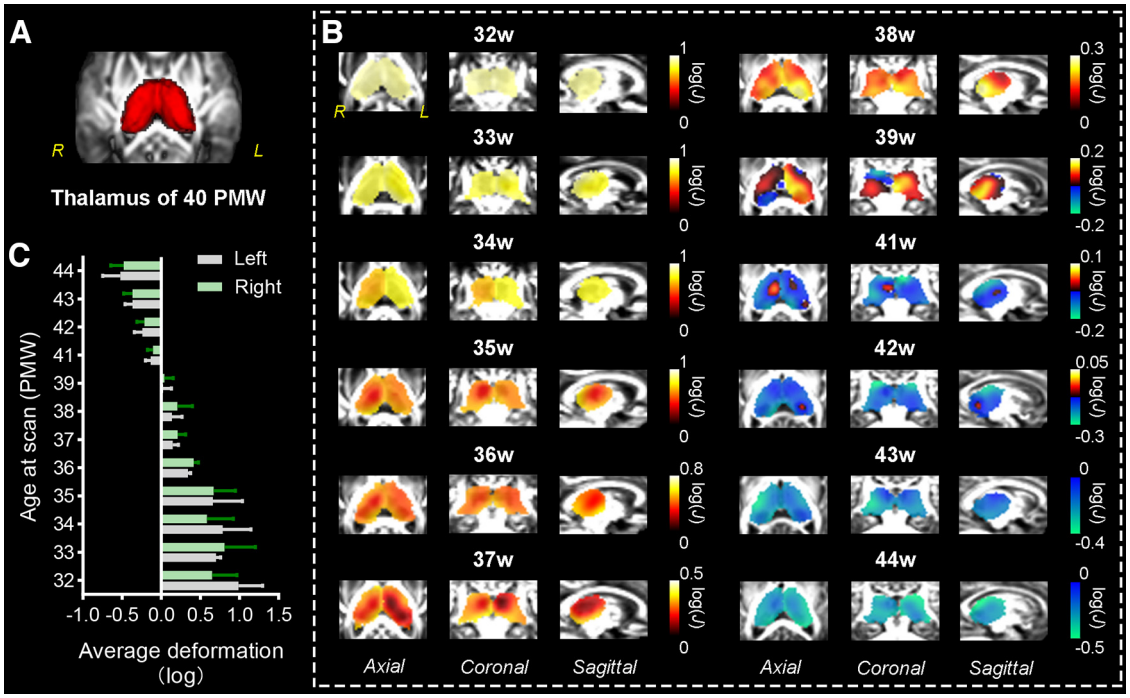

Figure 2. Morphologic development of the bilateral thalamus during 32–44 PMWs relative to the thalamus of 40 PMWs. ***A***, Visualization of the thalamus in the 40 PMWs template. ***B***, The extent of morphologic deformation of the thalamus at each PMW relative to the 40 PMWs template, as quantified by the logarithm of the *J* value of the transformation matrices. $J > 0$ indicate a morphologic expansion compared with the reference image and values < 0 indicate opposite changes. ***C***, Average deformation of left and right thalamus at each PMW. No significant laterality in deformation measurement was found during development (p values > 0.05, paired t test, FWE corrected).

postmenstrual age (PMA) at scan, and head circumference at scan with the PB-TEA (no significant differences in these demographics). The comparison between PB-AB and PB-TEA groups would serve as a validation for the first purpose and the comparison between PB-TEA and TB could be used for the second purpose. Basic information regarding the demographics of the validation dataset is shown in Table 2. For each group, thalamic microstructures (i.e., FA, FD, FC, MD, AD, and RD) and subdivisions, as well as thalamocortical connectivity, were obtained through the aforementioned approaches.

Statistical analysis

The generalized linear model was used to evaluate the correlations between PMA at the scan and structural metrics of the thalamus (Y), with gender, head circumference at scan, body weight at birth, and twin/singleton as covariates, as follows:

$$Y = \beta_0 + \beta_1 \times \mathrm{PMA} + \beta_2 \times \mathrm{gender} + \beta_3 \times \mathrm{head\_circumference} + \beta_4 \times \mathrm{weight} + \beta_5 \times \mathrm{singleton}.$$

For age correlation analysis, thalamic volume, mean microstructural metrics (i.e., FD, FA, FC, MD, AD, and RD), and their asymmetric index [calculated as (left – right)/(left + right)] were computed in the individual space as features. For fixel/voxel-level correlation analysis of these metrics, all the subjects were registered to the population FOD template to ensure spatial alignment across subjects. In validation analysis, we performed a paired t test to examine the difference of thalamic microstructures between PB-AB and PB-TEA groups. Analysis of covariance (ANCOVA), a multiple regression model with the aforementioned covariates, was used to evaluate the difference between PB-TEA and TB cohorts. The p values from fixel/voxel-level correlation analysis and multiple comparisons in validation analysis were corrected by using family-wise error (FWE) at the level of $p = 0.05$.

Data availability

The data that support the findings of this study are openly available at http://www.developingconnectome.org.

Results

Morphologic changes of the thalamus

Figure 2 illustrates the morphologic changes of the bilateral thalamus during 32–44 PMWs relative to the population template at 40 PMWs. Evident growth of the thalamus with age was observed, and the deformation pattern varied from week to week. Specifically, the whole thalamus enlarged drastically from 32 to 34 PMWs; then the growth rate slowed down and a spatial gradient of deformation pattern emerged. Specifically, the marginal area (e.g., ventrolateral and pulvinar parts) showed greater deformation than the central part, in 35- to 38-week-old neonates relative to 40 PMWs (Fig. 2*B*). The dorsal and ventral parts of the thalamus showed alternating rapid expansion from 42 to 44 PMWs. In addition, no significant laterality of shape changes was found between bilateral thalamus (p values > 0.05, paired t test, FWE corrected; Fig. 2*C*).

Development of thalamic microstructures

Regional metrics (i.e., volume and average microstructural metrics of the thalamus) were computed in the individual space. The volume, FA, and FD of bilateral thalamus significantly increased with age (r values > 0.39, p values < 0.0001; Fig. 3), whereas the diffusivity measures (i.e., MD, AD, and RD) showed opposite developmental trends (r values < -0.59, p values < 0.0001; Fig. 3). We also found that FA and FD showed rightward lateralization (higher values in the right thalamus; asymmetry index < 0), which is consistent with the lower diffusivity values on the right side, indicating higher structural maturity in the right thalamus. Moreover, the thalamic volume showed a shift of lateralization from leftward (higher volume on left) to rightward (higher volume on right), with the zero-crossing occurring around 40 PMWs. However, no significant correlation was found between the laterality of these metrics and PMA (p values > 0.05).

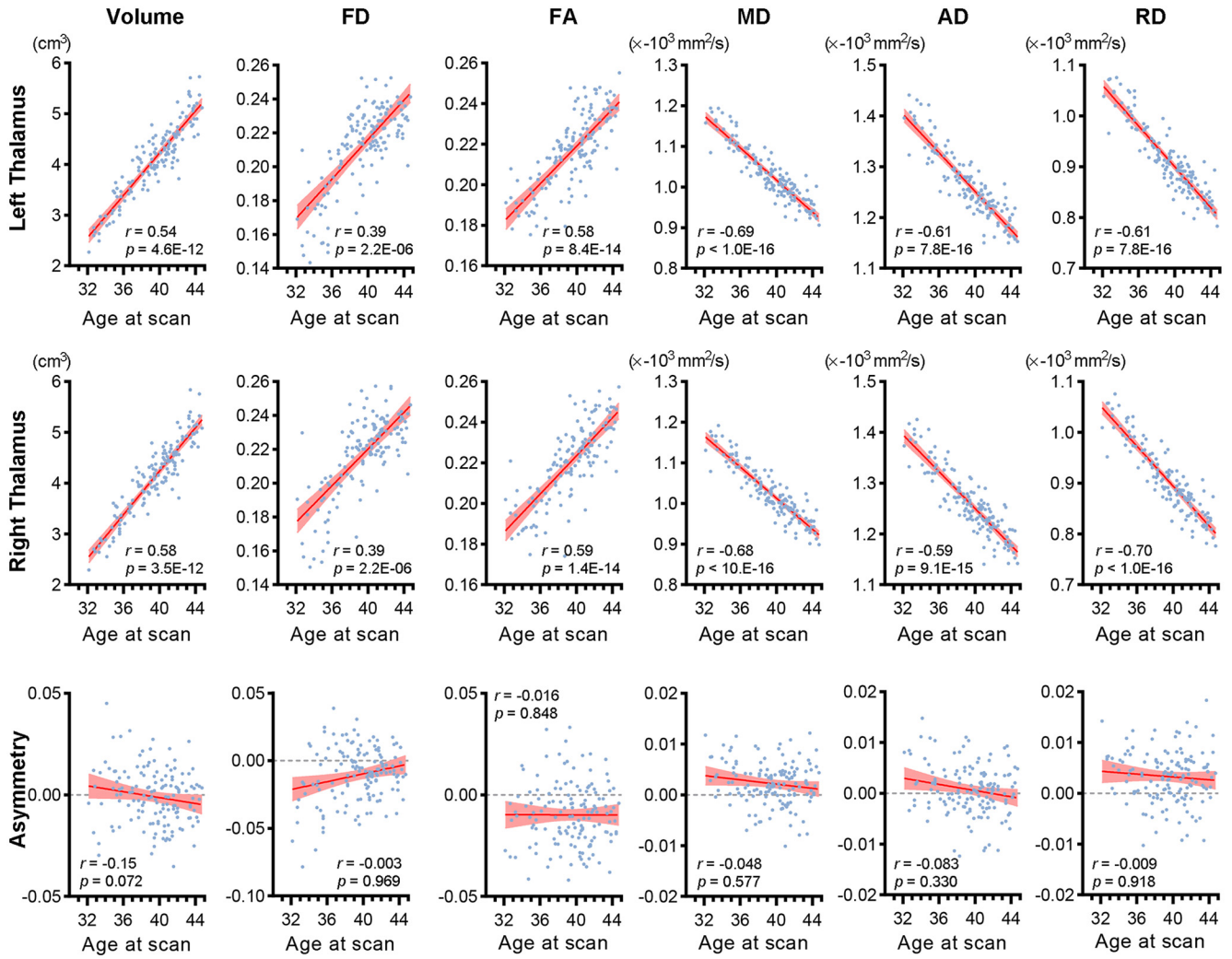

Figure 3. Developmental changes of the macrostructural and microstructural features of bilateral thalamus during 32–44 PMWs, including volume, FD, FA, MD, AD, and RD. These features were calculated in native dMRI space. Thalamic volume, FD, and FA significantly increased with PMA (r values $>$ 0.39, p values $<$ 0.0001), whereas the diffusivity indices (i.e., MD, AD, and RD) showed opposite trend (r values $<$ −0.59, p values $<$ 0.0001). The asymmetry of these metrics did not significantly correlate with PMA (last row). Note that an asymmetry index $>$0 indicates higher values in the left, and an index $<$0 indicates the opposite.

Similar developmental trends of these microstructures were also observed at the fixel/voxel level. As shown in Figure 4, increased fiber integrity (i.e., increased FA, FD, and FC) was accompanied by reduced diffusivity (i.e., MD, AD, and RD) with age in the majority of the thalamic voxels (p values $<$ 0.05, FWE corrected). Interestingly, these changes were more pronounced in the lateral thalamus (higher t-values), especially for FA and FD; whereas, the microstructures of ventromedial parts showed less association with age.

Development of thalamocortical fiber tracts

The developmental profile of thalamocortical fibers was delineated in Figure 5*A*. At 32 PMWs, fiber connecting the thalamus with corpus callosum, and temporal, parietal, and occipital cortices was observed, and the extent of connections increased with PMW. A thalamofrontal pathway that connects the thalamus to high-order functional domains emerged at ~40 PMWs or later (left, 40 PMWs; right 42 PMWs) and involved a lower proportion of fibers than pathways to other cortices (Fig. 5*B*). By projecting the thalamocortical fibers back to the thalamus, we found that voxels with high tract density initially appeared at the posterolateral side of the bilateral thalamus (pulvinar nuclei) and gradually overtook the head and central parts of the thalamus (Fig. 5*C*). This observation was congruent with the fast microstructural development in the lateral thalamus in Figure 4.

Formation of thalamic subdivisions

To investigate the functional development of thalamic subdivisions (e.g., how they innervate different cortical areas), we performed connectivity-based segmentation on the thalamus. The five identified subdivisions, spatially distributed along the anterior–posterior axis, were mainly connected with frontal (Fig. 6*A*, red), motor (Fig. 6*A*, yellow), somatosensory (Fig. 6*A*, orange), parietal-occipital (Fig. 6*A*, blue), and temporal (Fig. 6*A*, green) cortices. Such spatial distribution patterns showed high consistency with the Oxford Thalamic Connectivity Atlas derived from adult data (Fig. 6*A*, last column). We found that the subdivisions on the lateral side of thalamus formed earlier than the central part, consistent with the developmental pattern of microstructure and thalamocortical connectivity described above. For example, the identified subdivisions at 32 PMWs were only small clusters distributed on the lateral boundary of the thalamus; these subdivisions then underwent continuous outside-in expansion and voxel reassignment to form a whole-

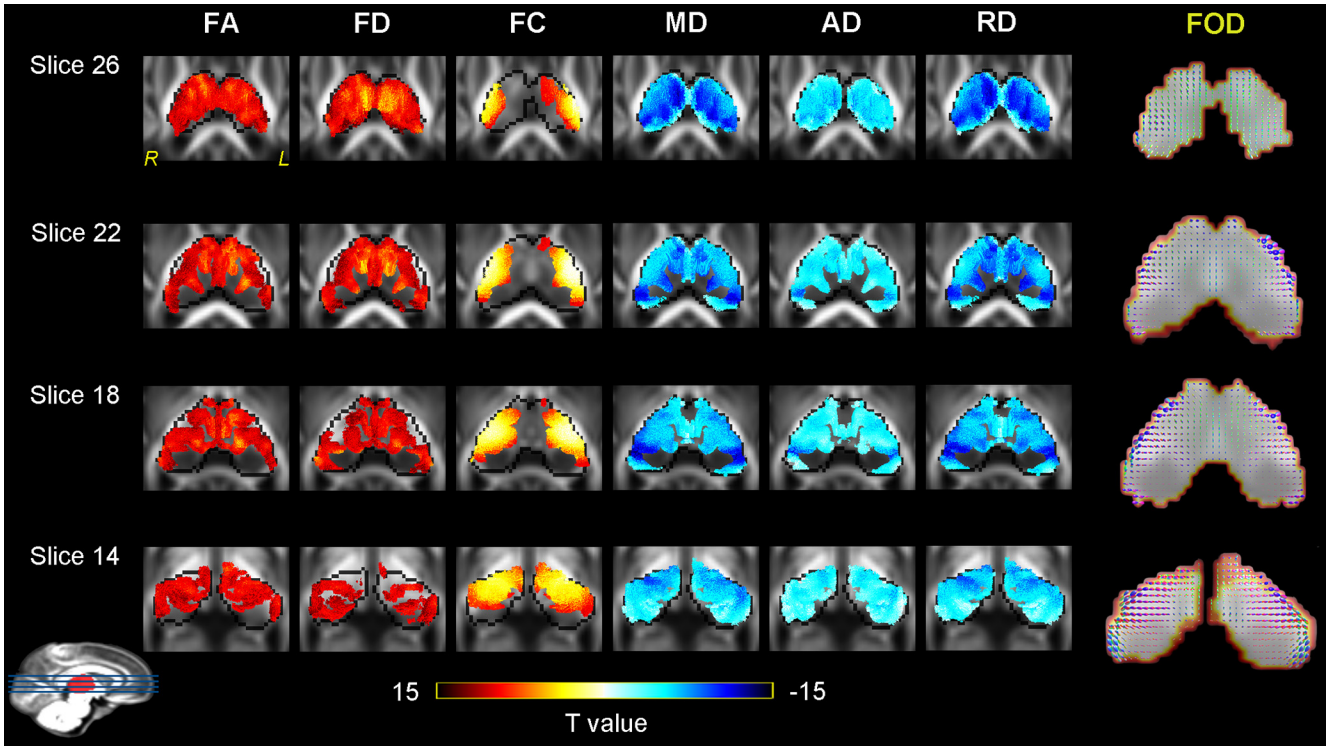

Figure 4. Correlation (in *t*-values) maps between PMA and the thalamic microstructural features, and the corresponding FOD maps in axial view at several slice locations. The correlation was calculated by registering all infant images to a population template space. FA, FD, and FC showed significant positive correlations with PMA, whereas diffusivity metrics showed negative correlations (p values < 0.05, FWE corrected). The *t*-values of the correlations were shown in the fixels/voxels with statistical significance.

thalamic parcellation. In addition, the thalamic subdivisions that connected to frontal and temporal cortices showed a larger size and faster growth than the other subdivisions (Fig. 6*C*).

Longitudinal development of thalamus and thalamocortical connectivity

We performed a validation analysis to examine our findings on an independent longitudinal dataset. There was a significant increase in the average FA, FD, and FC in left and right thalamus (paired t test, p values < 0.001), accompanied by reduced diffusivity (paired t test, p values < 0.001) during the development of thalamus from birth to TEA in PB neonates (Fig. 7*A*). No significant difference was found in these microstructural metrics between PB-TEA and TB infants (ANCOVA, p values > 0.05). The number of thalamocortical fibers rapidly increased from preterm birth to TEA, and the fiber tracts connecting to corpus callosum, and temporal, parietal, and occipital cortices were more pronounced than thalamofrontal connectivity at both time points (Fig. 7*B*). Compared with PB-TEA infants, the thalamocortical fiber tracts of TB infants showed a higher number of fibers and a more developed pathway between thalamus and frontal cortex (Fig. 7*B*). In addition, a similar developmental pattern of thalamic subdivisions was observed from preterm birth to TEA, including earlier development on the lateral side than the central part of thalamus and the lateral-to-medial formation order of the subdivisions, and no obvious difference between PB-TEA and TB was visually detected (Fig. 7*C*).

Discussion

The present study characterized the spatiotemporal developmental pattern of the thalamus in neonatal brains during 32–44 PMWs, from morphologic, microstructural, and connectome perspectives, using high-angular resolution dMRI data. Our results showed that thalamic development during this period exhibited (1) evident morphologic expansion, especially in the ventrolateral part; (2) later development of thalamocortical connection to frontal lobe than to the other lobes; and (3) a lateral-to-medial pattern for both microstructural development and formation of thalamic subdivisions. To the best of our knowledge, this is the first study that comprehensively depicted the developmental process of thalamus in perinatal human brains, which enriches our understanding of the developmental principles of thalamus and also provides references for the atypical brain growth in neurodevelopmental disorders.

Spatial gradient in thalamic morphologic development

Although previous studies (Makropoulos et al., 2016; Gui et al., 2019) have identified thalamic volume increases with age, our study extended these observations and showed heterogeneity in the deformation pattern of thalamic morphology at different postnatal stages. For example, morphologic changes were relatively uniform across the entire thalamus before 35 weeks PMA, and the deformation became more pronounced at the border than in the central part of thalamus afterward. Since the major cortical targets of ventral and centrolateral nuclei are sensorimotor cortices and prefrontal cortex, respectively (Behrens et al., 2003; Sherman and Guillery, 2013), faster expansion of ventral thalamus than the centrolateral parts may suggest earlier development of sensorimotor cortex than prefrontal cortex (Li et al., 2021). This result partially corresponded to a previous study indicating significant differences on the surface of anterior and ventral thalamic nuclei in PB infants at TEA compared with

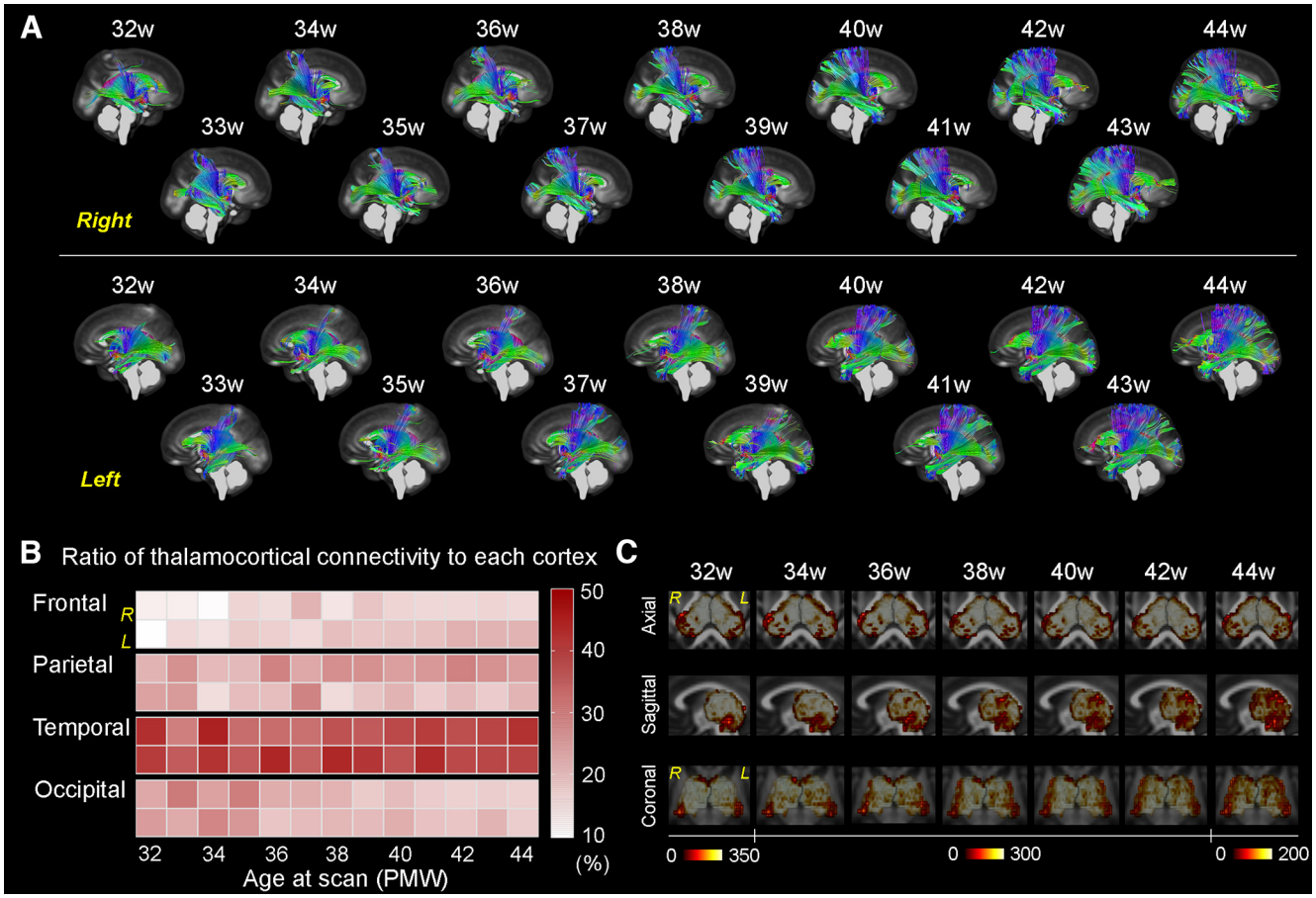

Figure 5. Development of thalamocortical connectivity during 32–44 PMWs. ***A***, Visualization of the thalamocortical fiber tracts at each PMW for the left and right hemispheres. ***B***, The ratio of streamlines between the thalamus and individual cortices (i.e., frontal, parietal, temporal, and occipital). The ratio was defined as the number of streamlines connected to each cortex divided by the total number of thalamocortical streamlines. ***C***, Density of thalamocortical fiber tracts in the thalamus. Note: results shown in this figure were computed based on the group template of each PMW.

term-born neonates (Lao et al., 2016), indicating that these rapidly developing regions may be more vulnerable to preterm birth.

In addition, though brain lateralization appears during the development from the second trimester of gestation to the first half-year after birth (Hering-Hanit et al., 2001; Corballis, 2013; Liu et al., 2021b), we did not find asymmetrical deformation patterns in thalamus during development. This was not surprising because the morphologic changes measured by the Jacobian determinant are of a relative magnitude that estimates the local expansion or contraction relative to the reference image, which may not capture the lateral difference if the asymmetry appears very early and bilateral nuclei grow at a similar rate.

Lateral-to-medial development of thalamic microstructure

The outward morphologic deformation and rapid increases of microstructural indices suggested simultaneous development of thalamus on both macroscopic and microscopic levels during this period. The linear increases of FA and FD and the decreases of diffusivity with PMA may correspond to the rapid growth of myelin content (e.g., oligodendrocytes proliferate) and the total amount of axons, suggesting increased fiber integrity within thalamus, and the results were in line with previous findings reported in term/preterm neonates (Paquette et al., 2015) and typical development from infancy to adulthood (McLaughlin et al., 2018). The rightward lateralization in FD and FA, and the shifting trend from leftward to rightward asymmetry in diffusivity metrics were in good accordance with our previous study indicating rightward asymmetry of the thalamus in dMRI measurements from TEA to 6 months (Liu et al., 2021b).

Interestingly, we noticed that the microstructural features of the lateral thalamus significantly correlated with PMA but not for the medial thalamus, suggesting a lateral-to-medial spatial pattern that microstructures developed faster in the lateral thalamus than those in the medial part during the perinatal period. Morel et al. (1997) have found that lateral and medial thalamus were characterized by immunoreactivity of different calcium-binding proteins (i.e., parvalbumin and calbindin D-28K). Because calcium is deeply involved in various aspects of neuronal differentiation, migration (Komuro and Kumada, 2005), and neurotransmitters expression (Spitzer, 1994), localization of these proteins may indicate differential neuronal populations and pathways in different regions (Andressen et al., 1993; Parent et al., 1996). Based on a guinea pig model, studies have revealed high expression of parvalbumin in laterodorsal thalamus at the prenatal stage (Zakowski et al., 2014), whereas calbindin D-28K was expressed in anteromedial thalamic nucleus after 20 d postnatally (Zakowski et al., 2013), which could possibly explain the earlier development of the lateral than the medial part of thalamus during the perinatal period.

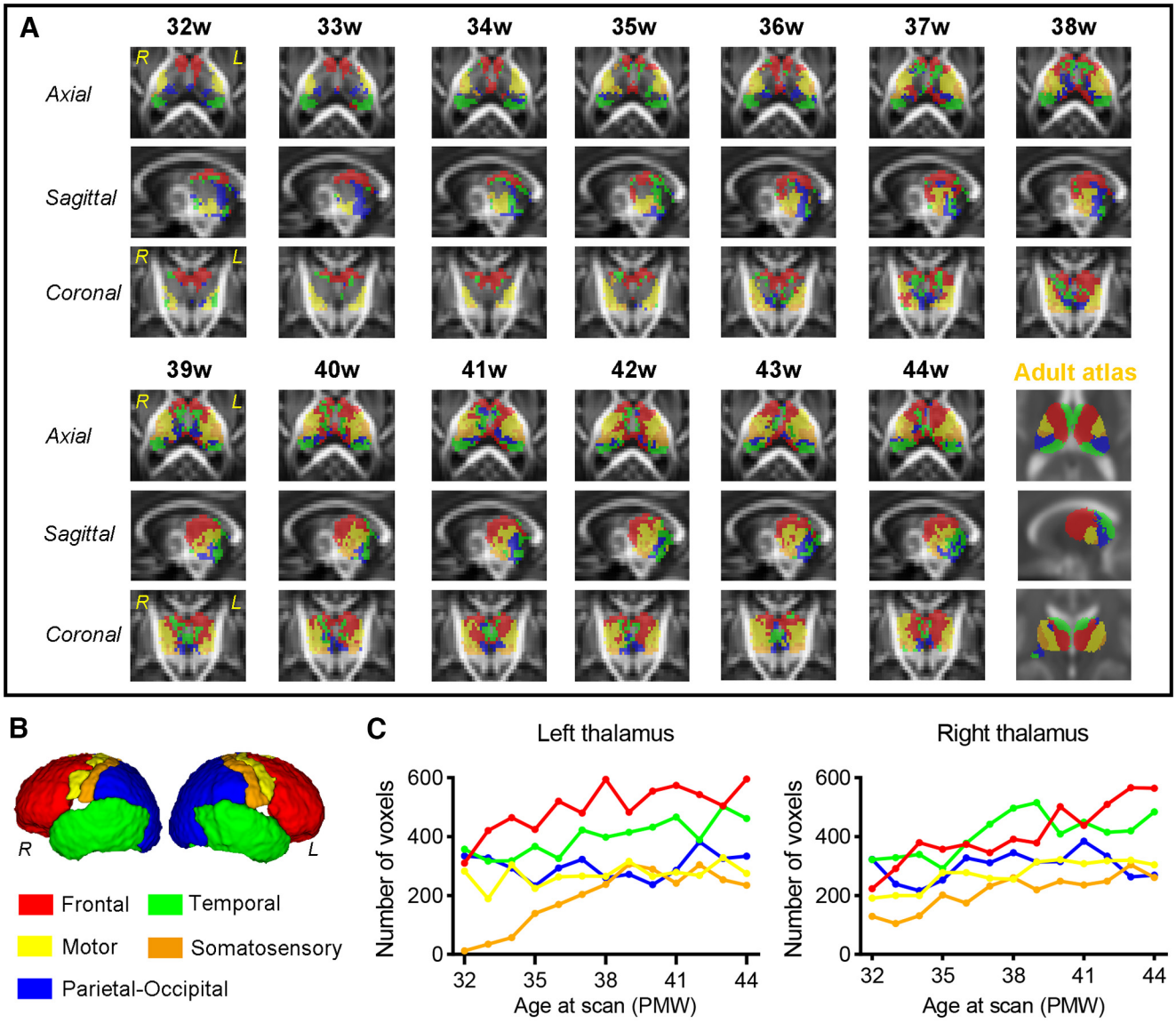

Figure 6. Development of thalamic subdivisions based on their connections to five cortical regions. ***A***, The thalamic subdivisions at each PMW were identified via a connectivity-based approach. The thalamic connectivity atlas of adults in MNI space was also given as a reference. ***B***, The five cortical seed regions that were used for thalamic nuclei segmentation, including frontal, temporal, motor, somatosensory, and parietal–occipital cortices. ***C***, Number of voxels within each thalamic subdivision during development. Note: results shown in this figure were computed based on the group template at each PMW.

Thalamocortical connectivity developed in a posterior–anterior order

The thalamofrontal connectivity pathway exhibited a lower extent of development compared with pathways linking the thalamus with the middle and posterior parts of the cortex. Moreover, by mapping the cortex-to-thalamus projection density on the thalamus, we found that the connected thalamic voxels spread along the lateral side of the thalamus from pulvinar nuclei that mainly connected with sensorimotor, visual, and temporal cortices at early stage, which later extended to more central and anterior parts that primarily connected with motor and prefrontal cortices (Nair et al., 2013; Zheng et al., 2021). These findings were congruent with the order of synaptic development that synaptic density peaks first in primary sensory cortex, followed by association areas and prefrontal cortex (Tau and Peterson, 2010). Furthermore, other studies have indicated that, by the end of full-term gestation, neurons have migrated to their targets in the frontal cortex (Paredes et al., 2016) and basic thalamocortical circuitry was established (Kostović and Jovanov-Milosević, 2006; Kostović and Judas, 2010), which could partly explain the emergence of detectable thalamofrontal connectivity at ~40 PMWs. The tract-density map of the thalamus was in good accordance with the developmental pattern of thalamic microstructures, and the rapid increases of axonal density and myelination in the lateral thalamus may contribute to the higher thalamocortical connections in these regions.

While there are multiple theories of thalamocortical axonal development (Crandall and Caviness, 1984; Agmon et al., 1993; Mitrofanis and Guillery, 1993; Métin and Godement, 1996; Molnár et al., 1998), one prominent theory—the "handshake" theory—posits that axonal pathways from the thalamus and cerebral cortex grow separately at the beginning and meet within the internal capsule (Métin and Godement, 1996; Molnár et al., 1998). Since the developmental order of synapse is from primary sensory cortex to high-order cortex (Tau and Peterson, 2010), we

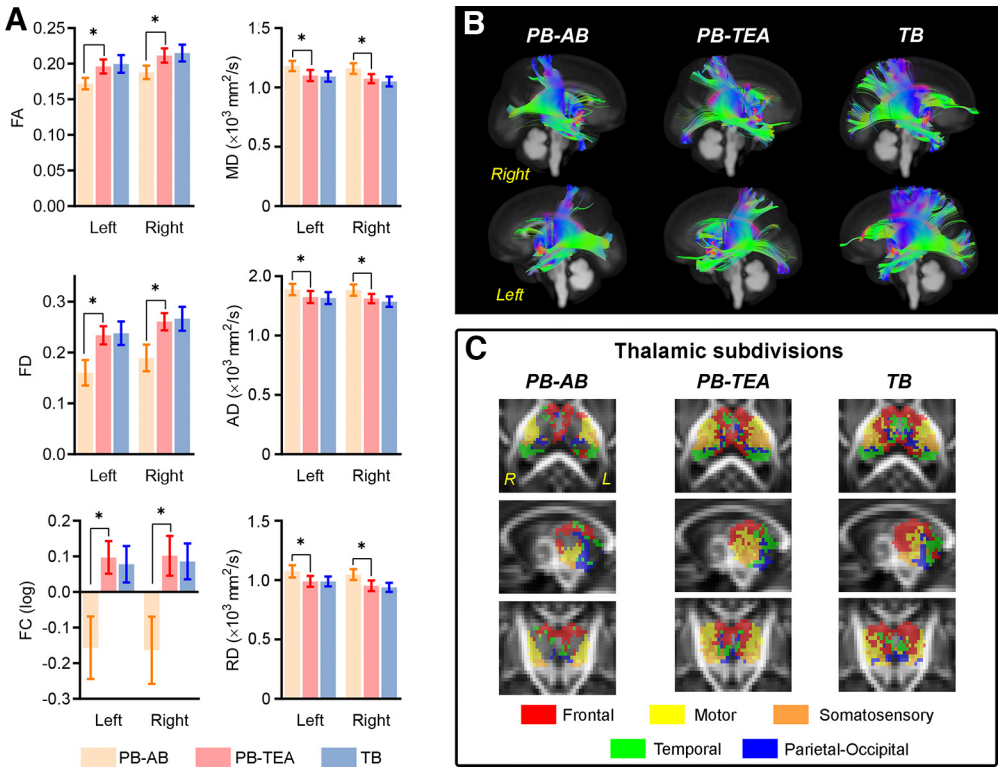

Figure 7. Comparisons of microstructures and subdivisions of the thalamus, and thalamocortical connectivity among PB-AB, PB-TEA, and TB infants. ***A***, Between-group differences in FA, FD, FC (log), MD, AD, and RD. Compared with PB-AB, PB-TEA showed significant increases of FA, FD, and FC (paired *t* test, *p* values < 0.05, FWE corrected), and significant decreases of diffusivity measures (paired *t* test, *p* values < 0.05, FWE corrected). No significant difference was found in these metrics between PB-TEA and TB (ANCOVA, *p* values > 0.05). No comparison was made between PB-AB and TB cohorts. ***B***, Visualization of the thalamocortical fiber tracts in the three groups for the left and right hemispheres. ***C***, The thalamic subdivisions in each group that were identified via a connectivity-based approach. Note: results shown in ***B*** and ***C*** were computed based on the FOD template of each group.

speculated that the fewer thalamofrontal connections might result from late axonal development in frontal cortex. This could also explain why the anterior projections from thalamus did not reach the cortex at early PMW. However, the delayed development of thalamofrontal connectivity might also be related to premature birth as observed in our validation data.

Subdivision of thalamus forms in a lateral-to-medial pattern

It has been reported that thalamic subdivisions segmented by thalamocortical connectivity corresponded well to histologically defined thalamic nuclei (Behrens et al., 2003). Since it is impossible to determine the boundaries of thalamic nuclei through histologic information *in vivo*, the connectivity-based approach might be an effective way to map the anatomic parcels within thalamus. The thalamic subdivisions we identified matched well with the connectivity-based parcellation of the thalamus in infants at term age, children, and young adults reported in previous literature (Behrens et al., 2003; Nair et al., 2013; Toulmin et al., 2015; Jaimes et al., 2018), suggesting that the specialized connection pattern has been established in the third trimester, as early as 32 PMWs. The development of connectivity-based thalamic subdivisions followed the same lateral-to-medial principle as observed in the microstructural and connectivity analysis, which might, to some extent, reflect the differentiation process of thalamic cytoarchitecture. Yet, we are aware that the cytoarchitecture-based thalamic parcellation can only be definitively determined postmortem, which may differ from the connectivity-based parcellation during brain development. Interestingly, the subdivisions connected to frontal and temporal cortices actively grew throughout the perinatal period observed in our study; whereas, the subdivisions associated with motor, somatosensory, and parietal-occipital lobes were maintained relatively unchanged after 38 PMWs, indicating that these subdivisions were already well established at birth. These findings were supported by a significant volumetric association between the thalamus and frontal/temporal lobes during early brain development (Ball et al., 2012; Makropoulos et al., 2016).

Notably, our results showed that, at ~40 PMWs, the subdivisions almost covered the entire thalamus, but the tract density maps in Figure 5*C* were not. These results were not in conflict because they derived from different fiber-tracking algorithms (i.e., deterministic tracking for thalamus-to-cortex projection and probabilistic tracking for cortex-to-thalamus projection and resultant nuclei segmentation). In this study, both deterministic and probabilistic tracking were FOD-based algorithms that were robust to crossing fiber effects (Tournier et al., 2010, 2012), but each approach has its advantages depending on the purposes. Specifically, the deterministic tractography provides high reliability in connectome mapping that can best recover the "ground-truth" connectivity for *in vivo* dMRI (Sarwar et al., 2019); whereas, the probabilistic method considers inherent uncertainty of fiber dispersion given the low anisotropy in cortical regions. The consistent developmental pattern identified by the two approaches suggested the robustness of our findings.

Limitation

A major limitation of the present study lies in the use of preterm-born infant brain MRI for mapping brain development, as the influences of preterm birth were unknown. Depicting the

developmental trajectory of the early human brain via combined preterm-born and term-born infant data have been commonly adopted in many previous studies (Ball et al., 2013a; Toulmin et al., 2015; Makropoulos et al., 2016; Cao et al., 2017; Ouyang et al., 2019; Zhao et al., 2019). Although the effects of extrauterine growth undoubtedly led to impaired development in microstructure (Ball et al., 2013a; Pannek et al., 2018; Ouyang et al., 2019; Dimitrova et al., 2021) and connectivity (Ball et al., 2012, 2013b; Pandit et al., 2014; Batalle et al., 2017; Liu et al., 2021a), these effects were considered to be much less pronounced compared with the developmental changes during the third trimester (Bourgeois et al., 1989; Kostović, 1990; Zhao et al., 2019). The comparable developmental extent of thalamic microstructures and subdivisions between PB-TEA and TB infants further supported this argument. Second, the cross-sectional dataset is unable to represent the real developmental trajectory of the thalamus. A longitudinal design is essential to remove the effects of individual differences in the early developmental period, which, however, is very difficult in practice. Third, because of the small number of preterm infants under 34 PMWs in the dHCP database after excluding brain injury and low-quality data, there were limited usable data for 32–34 PMWs, which might lead to high variability in brain template (Yang et al., 2020). Future studies on a larger, independent dataset are needed to validate findings from this work. In addition, the brain structure changes dramatically after birth, making the registration of neonatal brains particularly challenging. Here, we used a FOD-guided registration algorithm to improve registration accuracy using the high-dimensional data (Raffelt et al., 2011), yet the registration accuracy was not evaluated in comparison with other algorithms.

Conclusion

The present study investigated the spatiotemporal developmental pattern of the thalamus in preterm-born and term-born infants from 32 to 44 PMWs. We found that the thalamic development was characterized by a lateral-to-medial developmental gradient at both morphologic and microstructural levels; as well as a lateral-to-medial gradient for subdivision formation. Thalamocortical connectivity analysis revealed a posterior-to-anterior developmental order with the thalamofrontal connection established the latest at ~40 PMWs. These findings portray a comprehensive view of the thalamic development in the early human brain.

References

Agmon A, Yang LT, O'Dowd DK, Jones EG (1993) Organized growth of thalamocortical axons from the deep tier of terminations into layer IV of developing mouse barrel cortex. J Neurosci 13:5365–5382.

Andersson JLR, Skare S, Ashburner J (2003) How to correct susceptibility distortions in spin-echo echo-planar images: application to diffusion tensor imaging. Neuroimage 20:870–888.

Andersson JLR, Sotiropoulos SN (2016) An integrated approach to correction for off-resonance effects and subject movement in diffusion MR imaging. Neuroimage 125:1063–1078.

Andersson JLR, Graham MS, Drobnjak I, Zhang H, Filippini N, Bastiani M (2017) Towards a comprehensive framework for movement and distortion correction of diffusion MR images: within volume movement. Neuroimage 152:450–466.

Andressen C, Blümcke I, Celio MR (1993) Calcium-binding proteins: selective markers of nerve cells. Cell Tissue Res 271:181–208.

Ball G, Boardman JP, Rueckert D, Aljabar P, Arichi T, Merchant N, Gousias IS, Edwards AD, Counsell SJ (2012) The effect of preterm birth on thalamic and cortical development. Cereb Cortex 22:1016–1024.

Ball G, Srinivasan L, Aljabar P, Counsell SJ, Durighel G, Hajnal JV, Rutherford MA, Edwards AD (2013a) Development of cortical microstructure in the preterm human brain. Proc Natl Acad Sci U|S|A 110:9541–9546.

Ball G, Boardman JP, Aljabar P, Pandit A, Arichi T, Merchant N, Rueckert D, Edwards AD, Counsell SJ (2013b) The influence of preterm birth on the developing thalamocortical connectome. Cortex 49:1711–1721.

Ball G, Pazderova L, Chew A, Tusor N, Merchant N, Arichi T, Allsop JM, Cowan FM, Edwards AD, Counsell SJ (2015) Thalamocortical connectivity predicts cognition in children born preterm. Cereb Cortex 25:4310–4318.

Bastiani M, Cottaar M, Fitzgibbon SP, Suri S, Alfaro-Almagro F, Sotiropoulos SN, Jbabdi S, Andersson JLR (2019a) Automated quality control for within and between studies diffusion MRI data using a non-parametric framework for movement and distortion correction. Neuroimage 184:801–812.

Bastiani M, Andersson JLR, Cordero-Grande L, Murgasova M, Hutter J, Price AN, Makropoulos A, Fitzgibbon SP, Hughes E, Rueckert D, Victor S, Rutherford M, Edwards AD, Smith SM, Tournier J-D, Hajnal JV, Jbabdi S, Sotiropoulos SN (2019b) Automated processing pipeline for neonatal diffusion MRI in the developing Human Connectome Project. Neuroimage 185:750–763.

Batalle D, Hughes EJ, Zhang H, Tournier JD, Tusor N, Aljabar P, Wali L, Alexander DC, Hajnal JV, Nosarti C, Edwards AD, Counsell SJ (2017) Early development of structural networks and the impact of prematurity on brain connectivity. Neuroimage 149:379–392.

Behrens TEJ, Johansen-Berg H, Woolrich MW, Smith SM, Wheeler-Kingshott CAM, Boulby PA, Barker GJ, Sillery EL, Sheehan K, Ciccarelli O, Thompson AJ, Brady JM, Matthews PM (2003) Non-invasive mapping of connections between human thalamus and cortex using diffusion imaging. Nat Neurosci 6:750–757.

Bourgeois JP, Jastreboff PJ, Rakic P (1989) Synaptogenesis in visual cortex of normal and preterm monkeys: evidence for intrinsic regulation of synaptic overproduction. Proc Natl Acad Sci U|S|A 86:4297–4301.

Cao M, He Y, Dai Z, Liao X, Jeon T, Ouyang M, Chalak L, Bi Y, Rollins N, Dong Q, Huang H (2017) Early development of functional network segregation revealed by connectomic analysis of the preterm human brain. Cereb Cortex 27:1949–1963.

Corballis MC (2013) Early signs of brain asymmetry. Trends Cogn Sci 17:554–555.

Crandall JE, Caviness VS Jr (1984) Axon strata of the cerebral wall in embryonic mice. Brain Res 316:185–195.

Dimitrova R, et al. (2021) Preterm birth alters the development of cortical microstructure and morphology at term-equivalent age. Neuroimage 243:118488.

Dostrovsky JO (2000) Role of thalamus in pain. Prog Brain Res 129:245–257.

Feng L, Li H, Oishi K, Mishra V, Song L, Peng Q, Ouyang M, Wang J, Slinger M, Jeon T, Lee L, Heyne R, Chalak L, Peng Y, Liu S, Huang H (2019) Age-specific gray and white matter DTI atlas for human brain at 33, 36 and 39 postmenstrual weeks. Neuroimage 185:685–698.

Greve DN, Fischl B (2009) Accurate and robust brain image alignment using boundary-based registration. Neuroimage 48:63–72.

Gui L, Loukas S, Lazeyras F, Hüppi PS, Meskaldji DE, Borradori Tolsa C (2019) Longitudinal study of neonatal brain tissue volumes in preterm infants and their ability to predict neurodevelopmental outcome. Neuroimage 185:728–741.

Hering-Hanit R, Achiron R, Lipitz S, Achiron A (2001) Asymmetry of fetal cerebral hemispheres: in utero ultrasound study. Arch Dis Child Fetal Neonatal Ed 85:F194–196.

Huang H, Zhang J, Wakana S, Zhang W, Ren T, Richards LJ, Yarowsky P, Donohue P, Graham E, van Zijl PC, Mori S (2006) White and gray matter development in human fetal, newborn and pediatric brains. Neuroimage 33:27–38.

Huang H, Xue R, Zhang J, Ren T, Richards LJ, Yarowsky P, Miller MI, Mori S (2009) Anatomical characterization of human fetal brain development with diffusion tensor magnetic resonance imaging. J Neurosci 29:4263–4273.

Hughes EJ, Winchman T, Padormo F, Teixeira R, Wurie J, Sharma M, Fox M, Hutter J, Cordero-Grande L, Price AN, Allsop J, Bueno-Conde J, Tusor N, Arichi T, Edwards AD, Rutherford MA, Counsell SJ, Hajnal JV (2017) A dedicated neonatal brain imaging system. Magn Reson Med 78:794–804.

Jaimes C, Cheng HH, Soul J, Ferradal S, Rathi Y, Gagoski B, Newburger JW, Grant PE, Zöllei L (2018) Probabilistic tractography-based thalamic parcellation in healthy newborns and newborns with congenital heart disease. J Magn Reson Imaging 47:1626–1637.

Jaimes C, Machado-Rivas F, Afacan O, Khan S, Marami B, Ortinau CM, Rollins CK, Velasco-Annis C, Warfield SK, Gholipour A (2020) In vivo characterization of emerging white matter microstructure in the fetal brain in the third trimester. Hum Brain Mapp 41:3177–3185.

Jenkinson M, Bannister P, Brady M, Smith S (2002) Improved optimization for the robust and accurate linear registration and motion correction of brain images. Neuroimage 17:825–841.

Jeurissen B, Tournier JD, Dhollander T, Connelly A, Sijbers J (2014) Multi-tissue constrained spherical deconvolution for improved analysis of multi-shell diffusion MRI data. Neuroimage 103:411–426.

Komuro H, Kumada T (2005) Ca^{2+} transients control CNS neuronal migration. Cell Calcium 37:387–393.

Kostović I (1990) Structural and histochemical reorganization of the human prefrontal cortex during perinatal and postnatal life. Prog Brain Res 85:223–239.

Kostović I, Jovanov-Milosević N (2006) The development of cerebral connections during the first 20-45 weeks' gestation. Semin Fetal Neonatal Med 11:415–422.

Kostović I, Judas M (2010) The development of the subplate and thalamocortical connections in the human foetal brain. Acta Paediatr 99:1119–1127.

Kuklisova-Murgasova M, Quaghebeur G, Rutherford MA, Hajnal JV, Schnabel JA (2012) Reconstruction of fetal brain MRI with intensity matching and complete outlier removal. Med Image Anal 16:1550–1564.

Lao Y, Wang Y, Shi J, Ceschin R, Nelson MD, Panigrahy A, Leporé N (2016) Thalamic alterations in preterm neonates and their relation to ventral striatum disturbances revealed by a combined shape and pose analysis. Brain Struct Funct 221:487–506.

Li H, Yan G, Luo W, Liu T, Wang Y, Liu R, Zheng W, Zhang Y, Li K, Zhao L, Limperopoulos C, Zou Y, Wu D (2021) Mapping fetal brain development based on automated segmentation and 4D brain atlasing. Brain Struct Funct 226:1961–1972.

Liu T, Zhang H, You Y, Zheng W, Zhao Z, Liu T, Su X, Tian F, Zhang Y, Wu D (2021a) Brain developmental differences between preterm-born twins and singletons: a multi-modal MRI Study. Jpr 8:276–285.

Liu T, Gao F, Zheng W, You Y, Zhao Z, Lv Y, Chen W, Zhang H, Ji C, Wu D (2021b) Diffusion MRI of the infant brain reveals unique asymmetry patterns during the first-half-year of development. Neuroimage 242:118465.

Métin C, Godement P (1996) The ganglionic eminence may be an intermediate target for corticofugal and thalamocortical axons. J Neurosci 16:3219–3235.

Machado-Rivas F, Afacan O, Khan S, Marami B, Rollins CK, Ortinau C, Velasco-Annis C, Warfield SK, Gholipour A, Jaimes C (2021) Tractography of the cerebellar peduncles in second- and third-trimester fetuses. AJNR Am J Neuroradiol 42:194–200.

Makropoulos A, Gousias IS, Ledig C, Aljabar P, Serag A, Hajnal JV, Edwards AD, Counsell SJ, Rueckert D (2014) Automatic whole brain MRI segmentation of the developing neonatal brain. IEEE Trans Med Imaging 33:1818–1831.

Makropoulos A, Aljabar P, Wright R, Hüning B, Merchant N, Arichi T, Tusor N, Hajnal JV, Edwards AD, Counsell SJ, Rueckert D (2016) Regional growth and atlasing of the developing human brain. Neuroimage 125:456–478.

McLaughlin K, Travers BG, Dadalko OI, Dean DC 3rd, Tromp D, Adluru N, Destiche D, Freeman A, Prigge MD, Froehlich A, Duffield TC, Zielinski BA, Bigler ED, Lange N, Anderson JS, Alexander AL, Lainhart JE (2018) Longitudinal development of thalamic and internal capsule microstructure in autism spectrum disorder. Autism Res 11:450–462.

Mitrofanis J, Guillery RW (1993) New views of the thalamic reticular nucleus in the adult and the developing brain. Trends Neurosci 16:240–245.

Molnár Z, Adams R, Blakemore C (1998) Mechanisms underlying the early establishment of thalamocortical connections in the rat. J Neurosci 18:5723–5745.

Morel A, Magnin M, Jeanmonod D (1997) Multiarchitectonic and stereotactic atlas of the human thalamus. J Comp Neurol 387:588–630.

Mumford D (1991) On the computational architecture of the neocortex. I. The role of the thalamo-cortical loop. Biol Cybern 65:135–145.

Nair A, Treiber JM, Shukla DK, Shih P, Müller R-A (2013) Impaired thalamocortical connectivity in autism spectrum disorder: a study of functional and anatomical connectivity. Brain 136:1942–1955.

Ouyang M, Jeon T, Sotiras A, Peng Q, Mishra V, Halovanic C, Chen M, Chalak L, Rollins N, Roberts TPL, Davatzikos C, Huang H (2019) Differential cortical microstructural maturation in the preterm human brain with diffusion kurtosis and tensor imaging. Proc Natl Acad Sci U|S|A 116:4681–4688.

Pandit AS, Robinson E, Aljabar P, Ball G, Gousias IS, Wang Z, Hajnal JV, Rueckert D, Counsell SJ, Montana G, Edwards AD (2014) Whole-brain mapping of structural connectivity in infants reveals altered connection strength associated with growth and preterm birth. Cereb Cortex 24:2324–2333.

Pannek K, Fripp J, George JM, Fiori S, Colditz PB, Boyd RN, Rose SE (2018) Fixel-based analysis reveals alterations is brain microstructure and macrostructure of preterm-born infants at term equivalent age. NeuroImage Clin 18:51–59.

Paquette LB, Votava-Smith JK, Ceschin R, Nagasunder AC, Jackson HA, Blüml S, Wisnowski JL, Panigrahy A (2015) Abnormal development of thalamic microstructure in premature neonates with congenital heart disease. Pediatr Cardiol 36:960–969.

Paredes MF, James D, Gil-Perotin S, Kim H, Cotter JA, Ng C, Sandoval K, Rowitch DH, Xu D, McQuillen PS, Garcia-Verdugo JM, Huang EJ, Alvarez-Buylla A (2016) Extensive migration of young neurons into the infant human frontal lobe. Science 354:81.

Parent A, Fortin M, Côté PY, Cicchetti F (1996) Calcium-binding proteins in primate basal ganglia. Neurosci Res 25:309–334.

Raffelt D, Tournier JD, Fripp J, Crozier S, Connelly A, Salvado O (2011) Symmetric diffeomorphic registration of fibre orientation distributions. Neuroimage 56:1171–1180.

Raffelt D, Tournier J-D, Crozier S, Connelly A, Salvado O (2012) Reorientation of fiber orientation distributions using apodized point spread functions. Magn Reson Med 67:844–855.

Raffelt DA, Tournier JD, Smith RE, Vaughan DN, Jackson G, Ridgway GR, Connelly A (2017) Investigating white matter fibre density and morphology using fixel-based analysis. Neuroimage 144:58–73.

Sarwar T, Ramamohanarao K, Zalesky A (2019) Mapping connectomes with diffusion MRI: deterministic or probabilistic tractography? Magn Reson Med 81:1368–1384.

Sherman SM, Guillery RW (2013) Functional connections of cortical areas: a new view from the thalamus. Cambridge, MA: MIT.

Shi F, Yap PT, Wu G, Jia H, Gilmore JH, Lin W, Shen D (2011) Infant brain atlases from neonates to 1- and 2-year-olds. PLoS One 6:e18746.

Song JW, Mitchell PD, Kolasinski J, Ellen Grant P, Galaburda AM, Takahashi E (2015) Asymmetry of white matter pathways in developing human brains. Cereb Cortex 25:2883–2893.

Spitzer NC (1994) Spontaneous Ca2+ spikes and waves in embryonic neurons: signaling systems for differentiation. Trends Neurosci 17:115–118.

Takahashi E, Folkerth RD, Galaburda AM, Grant PE (2012) Emerging cerebral connectivity in the human fetal brain: an MR tractography study. Cereb Cortex 22:455–464.

Tau GZ, Peterson BS (2010) Normal development of brain circuits. Neuropsychopharmacology 35:147–168.

Torrico TJ, Munakomi S (2021) Neuroanatomy, thalamus. In: StatPearls. Treasure Island, FL: StatPearls Publishing.

Toulmin H, Beckmann CF, O'Muircheartaigh J, Ball G, Nongena P, Makropoulos A, Ederies A, Counsell SJ, Kennea N, Arichi T, Tusor N, Rutherford MA, Azzopardi D, Gonzalez-Cinca N, Hajnal JV, Edwards AD (2015) Specialization and integration of functional thalamocortical connectivity in the human infant. Proc Natl Acad Sci U|S|A 112:6485–6490.

Toulmin H, O'Muircheartaigh J, Counsell SJ, Falconer S, Chew A, Beckmann CF, Edwards AD (2021) Functional thalamocortical connectivity at term equivalent age and outcome at 2 years in infants born preterm. Cortex 135:17–29.

Tournier J-D, Calamante F, Connelly A (2010) Improved probabilistic streamlines tractography by 2nd order integration over fibre orientation distributions. Proc Intl Soc Mag Reson Med 18:1670.

Tournier J-D, Calamante F, Connelly A (2012) MRtrix: diffusion tractography in crossing fiber regions. Int J Imaging Syst Technol 22:53–66.

Vasung L, Huang H, Jovanov-Milošević N, Pletikos M, Mori S, Kostović I (2010) Development of axonal pathways in the human fetal fronto-limbic brain: histochemical characterization and diffusion tensor imaging. J Anat 217:400–417.

Ward LM (2011) The thalamic dynamic core theory of conscious experience. Conscious Cogn 20:464–486.

Ward LM (2013) The thalamus: gateway to the mind. Wiley Interdiscip Rev Cogn Sci 4:609–622.

Wilson S, Pietsch M, Cordero-Grande L, Price AN, Hutter J, Xiao J, McCabe L, Rutherford MA, Hughes EJ, Counsell SJ, Tournier JD, Arichi T, Hajnal JV, Edwards AD, Christiaens D, O'Muircheartaigh J (2021) Development of human white matter pathways in utero over the second and third trimester. Proc Natl Acad Sci U|S|A 118:e2023598118.

Yang G, Zhou S, Bozek J, Dong HM, Han M, Zuo XN, Liu H, Gao JH (2020) Sample sizes and population differences in brain template construction. Neuroimage 206:116318.

Zakowski W, Bogus-Nowakowska K, Robak A (2013) Embryonic and postnatal development of calcium-binding proteins immunoreactivity in the anterior thalamus of the guinea pig. J Chem Neuroanat 53:25–32.

Zakowski W, Bogus-Nowakowska K, Wasilewska B, Hermanowicz B, Robak A (2014) Calcium-binding proteins in the laterodorsal thalamic nucleus during development of the guinea pig. J Chem Neuroanat 61-62:88–93.

Zhao T, Mishra V, Jeon T, Ouyang M, Peng Q, Chalak L, Wisnowski JL, Heyne R, Rollins N, Shu N, Huang H (2019) Structural network maturation of the preterm human brain. Neuroimage 185:699–710.

Zheng W, Tan X, Liu T, Li X, Gao J, Hong L, Zhang X, Zhao Z, Yu Y, Zhang Y, Luo B, Wu D (2021) Individualized thalamic parcellation reveals alterations in shape and microstructure of thalamic nuclei in patients with disorder of consciousness. Cereb Cortex Commun 2:tgab024.